Electrical Power and Energy Systems 137 (2022) 107777

Contents lists available at ScienceDirect

International Journal of Electrical Power and Energy Systems

journal homepage: www.elsevier.com/locate/ijepes

# Forecasting intra-hour solar photovoltaic energy by assembling wavelet based time-frequency analysis with deep learning neural networks

Fermín Rodríguez *, Iñigo Azcárate, Javier Vadillo, Ainhoa Galarza

*Ceit-Basque Research and Technology Alliance (BRTA), Manuel Lardizabal 15, 20018 Donostia/San Sebastián, Spain*
*Universidad de Navarra, Tecnun, Manuel Lardizabal 13, 20018 Donostia/San Sebastián, Spain*

ARTICLE INFO

*Keywords:*
Photovoltaic generation
Solar irradiation
Time-frequency analysis
Artificial intelligence
Intra-hour forecasting

ABSTRACT

Due to the expected lack of fossil fuels in near future as well as climate change produced by greenhouse effect as consequence of environmental emissions, renewable energy generation, and specifically solar photovoltaic generation, has become relevant in present energy generation challenge. Photovoltaic generators have strong relationship with solar irradiation and outdoor temperature in energy generation process. These meteorological parameters are volatile and uncertain in nature so, unexpected changes on these parameters produce variations on solar photovoltaic generators' output power. While many researchers have been focused in recent years on the development of novel models for forecasting involved meteorological parameters in photovoltaic generation, they commonly do not consider an analysis step of the data before using it in the developed models. Hence, the aim of this study consists in assembling a wavelet based time-frequency analysis of the used data with deep learning neural networks to forecast solar irradiation, in next 10 min, to compute solar photovoltaic generation. Results of the validation step showed that the deviation of the proposed forecaster was lower than 4% in 90.60% of studied sample days. Final forecaster's root mean square error was 35.77 W/m$^2$, which was an accuracy improvement of 37.52% compared against persistence benchmark model.

## 1. Introduction

Along last century, and specifically in recent decades, electric power has been the key energy carrier to make it possible the evolution of modern societies at developed countries [1,2]. Although it is assumed a reduction of devices' power intensity based on an efficiency improvement in following years, different studies claim that this reduction through devices efficiency improvement will not be enough to stop electric power demand increasing trend [3]. Electric energy carriers rising evolution is based on the prediction of a higher electrified society where new electric devices such as full electric vehicles emerge [4,5]. In this scenario where an electric energy carrier is expected to continue growing up, combined with a shortage of fossil fuels as well as the climate change produced by the greenhouse effect emissions [6], renewable energy generation, and specifically solar photovoltaic (PV) generation, has become relevant in present energy generation challenge [7,8]. Nevertheless, to meet a high penetration of PV generation in traditional power grids, some challenges based on the intermittency of involved meteorological parameters in PV generation, mainly caused by clouds dynamic, need to be addressed. This intermittency of PV generation has effects on the demand-supply balance for guaranteeing power systems stability [9] as well as on the operation of electricity markets with additional production costs [10]. Therefore, transmission and distribution system operators ask to reduce renewable generators uncertainty level before continuing increasing the penetration level, to ensure power systems stability [11].

In recent years researchers have suggested different options in order to reduce renewable generators' uncertainty level. For instance, the combination of large-scale renewable generators with energy storage devices [12], the ensemble of small-scale renewable generators [13] or the development of better forecasters with higher accuracy [14]. Concerning renewable large-scale generators, power system operators suggest the introduction of large-scale storage systems, such as batteries, in order to ensure traditional grids' stability when unexpected power generation situations occur [15,16]. The merge of different renewable technologies, giving as a result the concept of virtual power plant, relies on the assumption that when some generators do not produce due to meteorological changes, other generators will be able to do it, in such way that the energy demand can be ensured with higher probability [12,13]. Although energy storage systems and virtual power plants will

* Corresponding author at: Ceit-Basque Research and Technology Alliance (BRTA), Manuel Lardizabal 15, 20018 Donostia/San Sebastián, Spain.
*E-mail addresses:* frlalanne@ceit.es (F. Rodríguez), a905290@alumni.unav.es (I. Azcárate), jvadillo@ceit.es (J. Vadillo), agalarza@ceit.es (A. Galarza).

https://doi.org/10.1016/j.ijepes.2021.107777
Received 27 August 2021; Received in revised form 13 October 2021; Accepted 4 November 2021
Available online 19 November 2021

help to reduce renewable generators' uncertainty level, the response of these systems is not immediate. This is the reason why many research works have support the idea of developing forecasters based on different techniques such as sky imagery or artificial intelligence to reduce renewable generators uncertainty level [17,18].

Developed forecasters related to meteorological parameters involved in solar PV generation are classified attending to two criterions: while first criterion examines proposed forecaster's prediction horizon, i.e. the time step between present and future effective of forecast [19], second criterion analyses proposed forecaster's technique. Concerning prediction horizon criterion, renewable forecasters are classified into following categories: a) intra-hour forecasters, b) intra-day forecasters and c) day-ahead forecasters [20,21]. Intra-hour forecasters, also noted in literature "nowcasting" [22,23] forecasters cover from few second to an hour ahead [24]. Thus, predictions obtained by these forecasters are used to ensure main grids stability through ancillary services dispatching [25]. Intra-day forecasters usually cover from one to six hours ahead [26,27] and their predictions are applied to ensure traditional grid's stability in zones with high penetration of renewable generators [28]. Finally, day-ahead forecasters cover from six to seventy-two hours ahead, usually with hourly resolution [29,30], and their predictions are applied for activities such as unit commitment or power reserve scheduling [31,32]. With respect to second criterion, developed forecasters are classified into physical, statistical or deep learning models attending on which technique has been used to develop proposed forecaster [21].

Physical models are in their turn categorised into: sky [24] or satellite imagery [33] and numerical weather prediction (NWP) models [28]. The selection of the model is done through the analysis of which are forecaster's spatial and temporal resolution parameters. For instance, while sky-imagery produces accurate predictions for intra-hour horizons and microscale spatial resolution [24], NWP is the best choice for day-ahead horizons and global spatial resolutions [28]. Sky and satellite imagery forecasters rely on the use of pictures to compute clouds motion-vectors, and through them predict future PV generation [24,33]. However, NWP forecasters are based on a depth understanding of the physical phenomena that takes places in the atmosphere to describe it through mathematical equations and combine it with numerical and differential computation [28,34]. Forecasters' development based on physical models is usually conditioned not only by the required depth understating of physical phenomena but also the expensive cost of involved devices to obtain the pictures [35]. Although there are big differences between statistical forecasters such as autoregressive moving average [36] or autoregressive integrated moving average [37] forecasters and deep learning models such as support vector machines [38] or neural networks [39], both statistical and deep learning models are based on time-series forecasting obtaining the relationships between involved features through historical databases [36-39]. Statistical and deep learning forecasters' main drawback is related to the necessity of big databases for being able to establish relationships between forecasters' output and chosen features [36,38]. Statistical models' main disadvantage against deep learning models rely on the fact that deep learning models are able to establish non-linear relationships between chosen features and forecasters' output [35,39], making them more reliable to predict unexpected changes of meteorological parameters involved in renewable generation [40].

A literature review indicates that researchers who currently based their forecasters on deep learning models are focussing their studies into following areas: a) available data pre-processing, b) the development of new models, c) hybridization of different models and finally d) computing of prediction intervals, with the purpose of increasing current forecasters accuracy as well as provide further information to power system decision makers. Available data pre-processing step bases on analysing and extracting the highest percentage of the information from the values of the selected features contained in the database. For instance, Shireen et al. [41] developed a Gaussian iterative multi-task process algorithm for those situations where it is needed to extend the information contained in PV databases. Proposed algorithm needs databases recorded under target location's similar meteorological conditions for being able to establish a relationship between target location's database and other locations' databases to extend the former. Likewise, Lan et al. [42] and Shing et al. [36] put their effort on identifying key features through principal component or time-series frequency analyses in order to reduce the number of features and extract from them the maximum information.

Concerning the development of new deep learning models, there are currently two main groups; while first group examines forecasters' accuracy improvement through the introduction of internal loops in the model, second group tries to emulate human's visual perception mechanism for pattern recognition and hence, increase forecasters' accuracy. For instance, long-short memory [43], gate-recurrent unit [40] and recurrent [39] neural networks are some examples of the widest examined models with the introduction of internal loops, whereas convolutional neural network (CNN) [44] model has been recently started to be analysed for renewable generation forecasting purposes based on the emulation of humans' visual recognition ability. CNN model relies on combining convolution and polling layers which contain kernel filters to extract patterns from databases to later compute the predictions [45]. Hybridization of different models relies on the assumption that the combination of different models will increase forecasters' accuracy. Due to the combination of different models, the computational cost is higher than on single models, so the hybridization is commonly used for intra-day horizons or longer [9,40]. Although there are several ways for models hybridization [46], the most usual ones are general ensemble and cluster ensemble hybrid models. While in general ensemble hybridization each of the combined models forecasts different features to compute in a second step the final prediction [47,48], in cluster ensemble hybridization, a previous step is done where databases' parameters with similar characteristics are previously clustered and then, general ensemble's same procedure is applied [49,50]. Finally, some researchers such as Li et al. [51] and Liu et al. [52] have started claiming that those traditional forecasters that only forecast single prediction point values do not provide complete information. Therefore, some research studies [51,53] suggest the computation through different ways of upper and lower confidence intervals around the prediction point to give further information to power systems controllers.

In this study, we make a pre-processing analysis of the solar irradiation information contained in available database throughout wavelet time-series frequency techniques. These techniques will provide solar irradiation original signal's frequencies in order to examine whether forecasters' accuracy can be improved with this information (see Fig. 1). Based on the microscale spatial resolution and 10 min temporal prediction horizon, each frequency obtained by each wavelet technique will be combined with a deep learning model whose parameters will be necessary to fix. The parameters that are involved in the input vectors of each deep learning model are: season, time of day and previous 24 h data with 10 min resolution. Therefore, 146 values are needed for each deep learning model to compute its prediction. Obtained solar irradiation predictions are used to compute solar PV generation 10 min-ahead. Key contributions of this study are:

1) The key contribution of this study relies on the development of a nowcasting solar irradiation forecaster, 10 min ahead, to compute PV output power. The forecaster relies on combining each time-series obtained from a wavelet frequency analysis of solar irradiation original signal with a deep learning neural network. In a second step, each neural network will make a prediction with the information provided by its associated frequency. Finally, it will be necessary to ensemble all predictions done by the neural networks to obtain final solar irradiation prediction value (see Fig. 1).

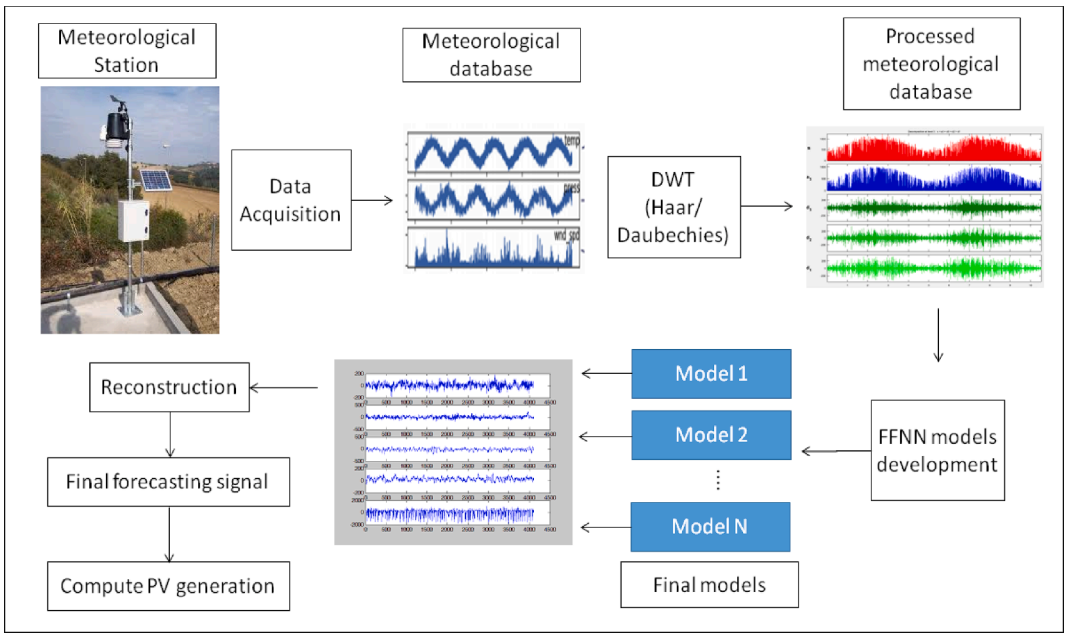


**Fig. 1.** Proposed solar irradiation model's flowchart.

2) Two different wavelet time-series frequency techniques, Haar and Daubechies, are examined in order to select the most accurate technique. Based on the results of a previous study [35] we have decided to combine obtained frequencies with feedforward neural networks whose internal parameters are necessary to fit. Moreover, root mean square error metric as well as other error metrics are computed to analyse proposed forecasters accuracy within the examined methods in this study, and also against results provided in literature.

The remainder of this paper is organised as follows. Section 2, examines wavelet time-series frequency theory and proposed forecaster's methodology. Section 3, provides the performance results of optimised proposed model, and those results are contrasted against literature ones for similar forecasting horizons. Present study's conclusions are in Section 4.

## 2. Methodology

The literature review done in above section demonstrates that, in recent years several nowcasting solar irradiation tools to compute PV output power have been examined. Due to proposed forecaster tries to reduce PV generators' uncertainty level in order to address these generators real-time control challenges, developed forecaster is categorized as intra-hour forecaster. To develop our forecaster, we first made Haar and Daubechies wavelet time-series frequency data pre-processing step analysis; then, each obtained frequency by the studied wavelet time-series frequency analyses is combined with a deep learning feedforward neural network, whose parameters were optimized by the methodology proposed in [35]. In addition, it has been decided to compute the persistence model as a benchmark in order to examine proposed model's accuracy improvement.

### 2.1. Examined wavelet time-series frequency analyses

Fourier transform (FT) is a mathematical concept which makes it possible to transform signals from temporal to frequency domains. Thus, through FT it is possible to obtain from an original temporal signal the decomposed frequency signals which it is made of. In the opposite way, through the inverse FT is possible to reconstruct from the decomposed frequency signals the original temporal signal. However, FT has the disadvantage of not reporting information about the time duration that each frequency is present in the original signal. In order to address this drawback, short time Fourier transform (STFT) was developed. STFT allows computing the FT in original signal's local sections. STFT for continuous signals is mathematically described as,

$$STFT\{x(t)\}(\sigma, w) \equiv X(\sigma, w) = \int_{-\infty}^{\infty} x(t)w(t-\sigma)e^{-jwt}dt \quad (1)$$

Where, $x(t)$ is the original function whose STFT is to be computed, $X(\sigma, w)$ is the FT of the $x(t)w(t-\sigma)$, a complex function which is used to represent the magnitude and phase of $x(t)$ over time and frequency, and finally, $e^{-jw}$ is Euler's formula. Nevertheless, taking into account Heisenberg's uncertainty principle, there is no chance to exactly determine which of the decomposed frequencies are present in a specific time. In addition, the STFT just provide information about the bands of the frequencies of $x(t)$ for an analysed lapse of time. Thus, the narrower the laps of time to get better time resolution of the original signal, the poorer the frequency resolution will be. This is the reason why time and frequency resolution need to be balance when STFT is decided to be applied.

The wavelet time-frequency transform proposed by Daubechies [54] is a feasible solution for STFT's compromise drawback to some extent. The calculation of continuous wavelet transform (CWT) is mathematically expressed in such way that,

$$CWT(a, b) = \int_{-\infty}^{\infty} x(t)\psi_{ab}(t)dt \quad (2)$$

Where $x(t)$ refers to the original continuous signal whose CWT is to be computed and $\psi_{ab}(t)$ is commonly noted in literature as mother wavelet. Hence, $CWT(a, b)$ coefficient for a certain scale ($a$ parameter) and translation ($b$ parameter) expresses the level of similarity between $x(t)$ and scaled and translated $\psi_{ab}(t)$. Thus, the set of all $CWT(a, b)$ coefficients of $x(t)$ is the wavelet representation with respect to $\psi_{ab}(t)$. Mother wavelet function must has time scalability and translation properties so it is mathematically defined as,

$$\psi_{ab}(t) = \frac{1}{\sqrt{a}}\psi\left(\frac{t-b}{a}\right) \quad (3)$$

The vast majority of the original signals that we can examined in the nature can be decomposed into low frequency components that appears along the full period of the signal and high frequency signals for little time lapses of the period. Therefore, the wavelet time-frequency transform was defined for being able to obtain good time and poor frequency resolutions for low scales and vice versa, for high scales.

Examined CWT works when analytical analyses are done, but it must be taken into account that when a signal is introduced in a computer for its numerical resolution, it must be discretized due to the fact that computers are only able to calculate CWT for a finite number of samples. Therefore, Eqs. (1) and (2) need to be redefined from continuous to discrete signals,

$$STFT\{x[(n)]\}(m,w) \equiv X(m,w) = \sum_{n=-\infty}^{\infty} x[n]w[n-m]e^{-jwn} \tag{4}$$

$$DWT(s,k) = \frac{1}{\sqrt{a_0^s}} \sum_{n=-\infty}^{\infty} x[n]\psi\left(\frac{n - kb_0a_0^s}{a_0^s}\right) \tag{5}$$

Where $x[n]$ refers to the discretized original signal $x(t)$, $n$ is the discrete time index of time $t$, $w[n]$ represents the examined lapse of time and $m$ and $w$ are discrete and quantized parameters by the assumption that analysed STFT is being calculated in a computer through the fast FT. Moreover, $k$ is an integer which refers to a particular point of $x[n]$ and $a$ and $b$ parameters of Eq. (3) are taken as a function of $s$ ($a = a_0^s$, $b = kb_0a_0^s$). For instance, in the case that we want to compute the series of binary wavelets, $a_0 = 2$ and $b_0 = 1$, in such way that Eq. (5) is expressed as,

$$DWT(s,k) = \frac{1}{\sqrt{2^s}} \sum_{n=-\infty}^{\infty} x[n]\psi(\frac{n - k2^s}{2^s})s, k = 0, \pm1, \pm2, \cdots. \tag{6}$$

Taking into account the following considerations: a) DWT provides enough information about the original continuous signal, b) examined discretized version of the CWT has a large computational cost and c) it is possible to compute wavelet coefficients by the use of algebraic convolutional-based equations. For this second way of computing the DWT, which is based on the pyramid algorithm, it is necessary to use high and low pass decomposition filters to separate the bands of frequencies present in $x[n]$ signal. In each level of the pyramid algorithm, the input signal to the $i$ th level is first passed through a low pass filter to obtain the approximation series, $a(i)$, and then, same input signal is passed through a high pass filter to obtain the detailed series, $d(i)$. The way for obtaining $a(i)$ and $d(i)$ for the first level of the pyramid is explained.

To compute the DWT of $x[n]$ signal, samples are passed through a low pass filter whose response impulse is noted by $g_1$ obtaining the convolution of both signals, that is expressed in such way that,

$$a1[n] = (x^*g_1)[n] = \sum_{k=-\infty}^{\infty} x[k]^*g_1[n-k] \tag{7}$$

Then, same $x[n]$ signal's samples are passed through a high pass filter whose response impulse is noted by $h_1$ obtaining the convolution of both signals, that is expressed in such way that,

$$d1[n] = (x^*h_1)[n] = \sum_{k=-\infty}^{\infty} x[k]^*h_1[n-k] \tag{8}$$

Both high and low pass filters have a quadrature mirror filter relationship.

The decomposition done to obtain pyramid's algorithm first level approximation and detailed series, $a1$ and $d1$, respectively can be further done to increase frequency resolution applying high and low pass filters into a1 approximation series. As it can be seen in Fig. 2, high and low pass filter are applied into previous levels approximation series.

Therefore, the original signal $x[n]$ can be reconstructed by the combination approximation and detailed series in such way that,

$$x[n] = a(I) + \sum_{i=1}^{I} d(i) \tag{11}$$

Where $a(I)$ is last computed pyramid's level approximation series, $I$ represents the total number of examined levels and $d(i)$ is the detailed series in the $i$th level. Therefore, in this second way of computing the DWT, the high and low pass filters that applied in each level of the pyramid algorithm have to be defined. In this study, available solar irradiation database contains discrete information with 10 min resolution so, for the data pre-processing step the second DWT method has been chosen based on its lower computational cost. In order to define high and low pass filters, two different strategies Haar and Daubechies DWT were examined.

### 2.2. Examined prediction models

#### 2.2.1. Persistence model

Nowcasting forecasters which are based on persistence model are easy to program. This is the reason why these models are usually computed in research studies to use them as benchmarks and examine novel forecaster accuracy performance. Persistence model assumes that, during the chosen time lapse between present moment and forecasting horizon time, the value of the parameter that is desired to predict will not change. This assumption is mathematically expressed as,

$$W(t+h) = W(t) \tag{12}$$

where $t$ represents present moment, $W(t)$ is predicted parameter's real

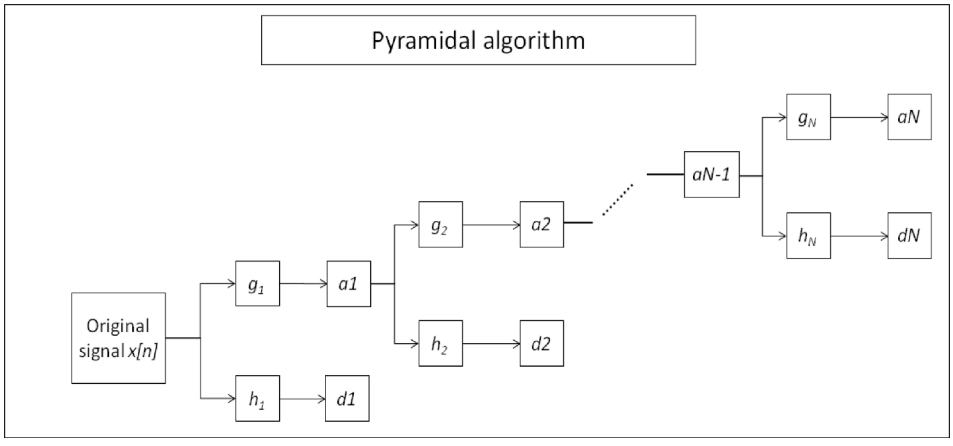


**Fig. 2.** Pyramid algorithm layout.

value at time $t$, $h$ refers to selected prediction horizon and $W(t+h)$ is the forecast done of chosen parameter at time $t+h$.

Meteorological parameters involved in renewable generation have strong relationships between them if chosen $h$ is small. Thus, for intra-hour forecasters, where the prediction horizon covers from few seconds to an hour ahead, the correlation gets stronger, so the accuracy of the model also increases. This model bases on using a present value to forecast the desired parameter, but its accuracy decreases when sudden changes must be predict.

#### 2.2.2. Deep learning models

Deep learning models' development has been based on the combination of mathematical algorithms noted in literature as learning algorithms and the emulation of human's brain memory or human's visual perception mechanism. Feedforward, recurrent, or long-short term memory neural networks models rely on the emulation of human's brain memory ability through a mathematical architecture. Convolution models rely on using a set of filters in each programmed convolution layer in order to extract patterns to make future prediction in such way to emulate human visual perception mechanism. Therefore, there is similarity between neural networks' neurons and convolution models' filters. Although researchers have traditionally developed forecasters based on neural networks for regressive forecasters [39,40,43] and convolutional models for image pattern recognition [54], some researchers have recently started to examine convolution methodology for regressive forecasters [45]. In a previous study with same data [35], we obtained, among different computed regressive forecasters, that feed-forward neural network (FFNN) model had the best accuracy for chosen prediction horizon, 10 min. Thus, FFNN model will be combined with the information obtained through the DWT analysis done in the data pre-processing step to examine whether the data pre-processing step increases the accuracy of the forecaster developed in a previous study [35].

FFNNs with recurrent and long short-term memory neural networks are probably the most analysed and computed models. In these models, there is a set of parameters that need to be selected, the common parameters for all mentioned models are training algorithm, model's number of layers, number of neurons per layer. FFNN model's main advantages rely on easier coding, lower number of parameters that need to be chosen, quicker training process and robustness when there is missing or abnormal data. Further information of FFNNs and other type of neural networks can be found at [55,56].

### 2.3. Proposed model

The nowcasting model presented in this paper consists on the combination of the detailed and approximation series obtained through the application of Haar and Daubechies DWTs to the available solar irradiation database with deep learning FFNN models. The main steps done to develop this model can be described as follow: first, Haar and Daubechies DWT strategies were applied to the solar irradiation training database in order to obtain solar irradiation's approximation $a(I)$ and detailed series $d(1)$ to $d(I)$. Then, for the series of each DWT strategy a FFNN model was developed. In order to fix the parameters of each FFNN in the learning step, the iterative methodology proposed in [35] was applied. Once the FFNN models are developed, it must be kept in mind that each FFNN model only provides a prediction for its approximation or detailed series, so Eq. (11) has to be applied in order to ensemble single predictions of each FFNN model to obtain final solar irradiation prediction. Finally, obtained solar irradiation predictions through presented model are applied following the methodology proposed by Ayvazoğluyüksel et al.'s [5] to compute PV output power generation. Although both Haar and Daubechies DWT strategies will be computed in order to examine which one obtains better accuracy on solar irradiation prediction, the PV output power generation prediction will only be run with the best strategy (see Fig. 1).

### 2.4. Error metrics

Mean absolute error (MAE), root mean square error (RMSE) and R-squared ($R^2$) are the most computed error metrics in forecasters literature [20,27,35,47] to compare new developed forecasters accuracy against literature results. While only RMSE and $R^2$ error metrics have been used to compare computed models accuracy, all error metrics have been used to compare final forecasters' accuracy against literature results. MAE, RMSE and $R^2$ error metric are mathematically expressed in such way that,

$$MAE = \frac{1}{N}\sum_{n=1}^{N}\left|Y_n - Y_n^{'}\right| \tag{13}$$

$$RMSE = \sqrt{\frac{1}{N}\sum_{n=1}^{N}\left(Y_n - Y_n^{'}\right)^2} \tag{14}$$

$$R^2 = 1 - \frac{\sum_{n=1}^{N}\left(Y_n - Y_n^{'}\right)^2}{\sum_{n=1}^{N}\left(Y_n - \overline{Y}\right)^2} \tag{15}$$

Where $Y_i$ is actual value; $Y_i^{'}$ is the prediction done by the forecaster, $N$ is the number of examined samples and $\overline{Y}$ is the average value of the $N$ predictions done.

## 3. Numerical results and discussion

In this research the database provided by Euskalmet, Basque Government's Meteorological Agency (http://www.euskalmet.euskadi.eus), has been used to compute examined models. To analyse proposed forecasters' accuracy, data from Vitoria-Gasteiz, which is the capital of the Basque Country, has been chosen. This database contains information from years 2015 to 2017 with 10 min resolution. The information of years 2015 and 2016 was used to the models' training step, while information of year 2017 has been used for the validation step, in order to ensure that proposed models have not previously seen validation step's data. Data pre-processing steps and computed models were done through MATLAB®.

### 3.1. Results for the models presented in Section 2

#### 3.1.1. Persistence model

Based on the difference between actual and predicted solar irradiation values, RMSE and $R^2$ error metrics were computed for the training and validation steps. While the RMSE for training and validation steps are 59.47 W/m$^2$ and 57.25 W/m$^2$, respectively, $R^2$ values are 0.9446 and 0.9518, respectively. Although it is not very usual to obtain worse accuracy error metrics in training step than in validation step, this fact relies on the fact that the meteorological information of the training database has bigger variance than validation step's database. Thus, it is expected that this trend where the validation results are better than trainings ones will be maintained through all the paper. Fig. 3 presents the solar irradiation evolution for actual and predicted values for a chosen random day of the validation dataset, June 16, 2017. While actual values are given by blue line, predicted values are given by orange one. Although it can be seen how prediction line is able to follow actual linés trend, the delay between both lines due to the assumption done by persistence model explained in Eq. (12) is demonstrated. The RMSE and $R^2$ values for June 16, 2017 day are 35.90 W/m$^2$ and 0.9903, respectively.

Moreover, RMSE and $R^2$ values computed for training and validation databases will be used as baseline to examine other computed forecasters performance. New proposed models accuracy improvement will be computed as,

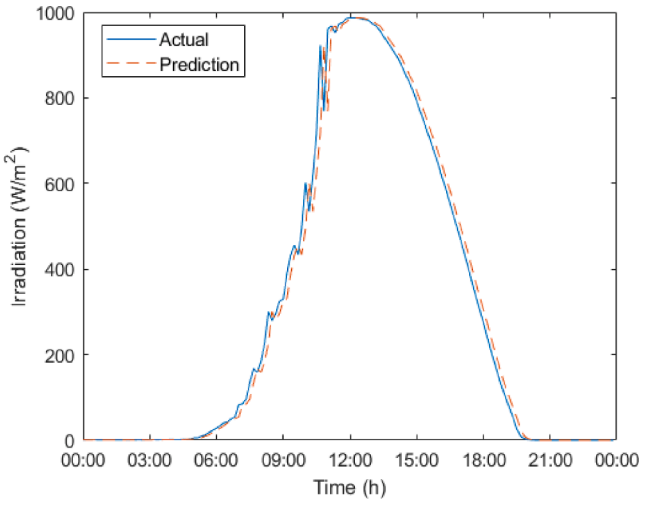


**Fig. 3.** Actual (blue) and forecasted (orange) values for June 16, 2017. (For interpretation of the references to colour in this figure legend, the reader is referred to the web version of this article.)

$$\text{Improvement}(\%) = \frac{RMSE_{baseline} - RMSE_{model}}{RMSE_{baseline}} * 100 \quad (16)$$

where $RMSE_{baseline}$ is the RMSE value computed through the persistence model, and $RMSE_{model}$ refers to proposed new models' RMSE. This improvement quantification is not only done for RMSE metric but also for $R^2$ metric with both databases, training and validation.

### 3.1.2. Feedforward neural network

In a previous study [35] where same database and prediction horizon were chosen, 10 min ahead, a 3-layer FFNN trained with Levenberg-Marquardt algorithm demonstrates to perform best. In the first layer, chosen input parameters are introduced to the model; in the second layer, neurons make the internal calculations; and finally, in the third layer, output value is obtained. In present research, same input vector as the one applied in [35] was used. This vector contains the following information: season, time of day and previous 24 h solar irradiation data with 10 min resolution, i.e., 146 values. Therefore, the purpose of this study is to follow the procedure developed in [35] to fix the neurons of FFNNs for each of the frequencies obtained through Haar and Daubechies wavelet time-frequency analysis and examine accuracy's evolution. In this study, a configuration which consists of an approximation and three detailed series, was selected for both wavelet time-frequency analyses. However, in future studies forecasters' accuracy evolution will be examined when these parameters are optimized.

*3.1.2.1. Haar wavelet time-frequency analysis.* Table 1 to 4 show the optimized FFNN model for each of the time-frequency series obtained through Haar analysis. RMSE and $R^2$ metrics were computed for training and validation datasets.

As it can be seen in Tables 1 and 2, best accuracy error metrics are obtained for same number of neurons in both databases. While in Table 1 FFNN structure with 20 neurons in the hidden layer produces best error metrics for approximation series $a(3)$, Table 2 shows that FFNN structure with 5 neurons in the hidden layer produces best error metrics for detail series $d(1)$. However, if Tables 3 and 4 are analysed it can be seen that different structures get best accuracy error metrics depending on the examined database. For instance, for detail series $d(2)$, 20 neurons FFNN structure makes best predictions with training database but 10 neurons FFNN structure makes best predictions for validation step. Therefore, taking into account that a forecaster is expected to work with previously unseen data, those structures that minimizes the RMSE and maximizes the R2 structures in the validation step will be chosen for the final forecaster.

Finally, after the combination of the predictions provided by the optimized structures of each approximation and detail series, proposed forecaster's accuracy error metrics were examined. With regards to the RMSE, proposed model improves from 59.47 W/m$^2$ to 36.80 W/m$^2$ in the training step and from 57.25 W/m$^2$ to 35.81 W/m$^2$ in the validation step. In terms of RMSE evolution it means an improvement of 38.12% and 37.47%, respectively. Concerning the $R^2$ error metric, the evolution was from 0.9446 to 0.9788 and 0.9518 to 0.9812 in learning and validation databases, respectively. Fig. 4 shows the evolution of solar irradiation's actual and forecasted values for June 16, 2017 for the proposed forecaster with Haar wavelet transform. While the RMSE calculated for this sample day was 31.70 W/m$^2$; which means an accuracy improvement of 11.70% compared against the persistence model, the $R^2$ error metric improves from 0.9903 to 0.9922.

*3.1.2.2. Daubechies wavelet time-frequency analysis.* Table 5 to 8 show the optimized FFNN model for each of the time-frequency series obtained through Daubechies analysis. RMSE and $R^2$ metrics were computed for training and validation datasets.

As it happens in Tables 3 and 4, from Table 5 to 8 once again different structures get best accuracy error metrics depending on the examined database. Based on previously given reason that forecasters are expected to work with previously unseen data, those structures that minimizes the

**Table 1**
Model's results for training and validation steps with approximation series $a(3)$.

| Configuration | Neurons | RMSE train. (W/m$^2$) | RMSE val. (W/m$^2$) | $R^2$ train. (–) | $R^2$ val. (–) |
|---|---|---|---|---|---|
| 1 | 5 | 27.84 | 27.42 | 0.9871 | 0.9883 |
| 2 | 10 | 27.57 | 27.41 | 0.9874 | 0.9884 |
| 3 | 15 | 27.38 | 27.41 | 0.9875 | 0.9884 |
| 4 | **20** | **27.31** | **27.32** | **0.9876** | **0.9885** |

**Table 2**
Model's results for training and validation steps with detail series $d(1)$.

| Configuration | Neurons | RMSE train. (W/m$^2$) | RMSE val. (W/m$^2$) | $R^2$ train. (–) | $R^2$ val. (–) |
|---|---|---|---|---|---|
| 1 | **5** | **29.32** | **28.49** | **0.0211** | **0.0059** |
| 2 | 10 | 29.37 | 28.52 | 0.0173 | 0.0034 |
| 3 | 15 | 29.41 | 28.59 | 0.0150 | 0.0017 |
| 4 | 20 | 29.41 | 28.60 | 0.0151 | 0.0016 |

**Table 3**
Model's results for training and validation steps with detail series $d(2)$.

| Configuration | Neurons | RMSE train. (W/m$^2$) | RMSE val. (W/m$^2$) | $R^2$ train. (–) | $R^2$ val. (–) |
|---|---|---|---|---|---|
| 1 | 5 | 23.84 | 22.40 | 0.4933 | 0.4802 |
| 2 | **10** | 23.71 | **22.38** | 0.4984 | **0.4809** |
| 3 | 15 | 23.66 | 22.46 | 0.5001 | 0.4773 |
| 4 | 20 | **23.62** | 22.58 | **0.5024** | 0.4717 |

**Table 4**
Model's results for training and validation steps with detail series $d(3)$.

| Configuration | Neurons | RMSE train. (W/m$^2$) | RMSE val. (W/m$^2$) | $R^2$ train. (–) | $R^2$ val. (–) |
|---|---|---|---|---|---|
| 1 | 5 | 19.72 | 20.02 | 0.7522 | 0.7467 |
| 2 | **10** | 19.51 | **19.96** | 0.7576 | **0.7482** |
| 3 | 15 | 19.45 | 20.02 | 0.7590 | 0.7468 |
| 4 | 20 | **19.40** | 20.03 | **0.7600** | 0.7465 |

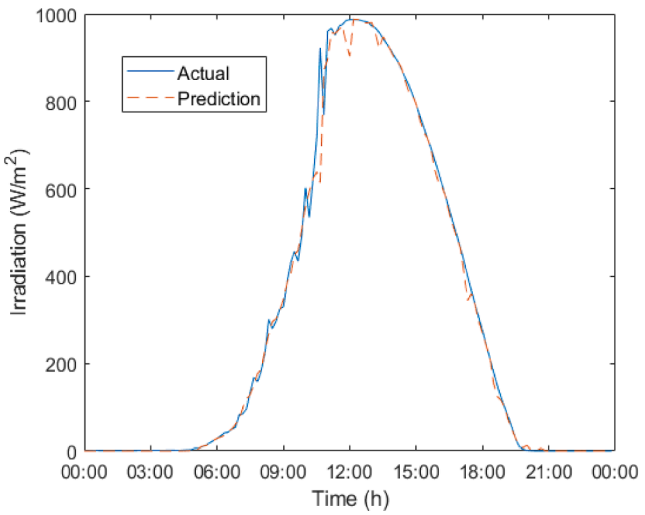


**Fig. 4.** Actual and forecasted values for June 16, 2017.

**Table 5**
Model's results for training and validation steps with approximation series $a(3)$.

| Configuration | Neurons | RMSE train. (W/m$^2$) | RMSE val. (W/m$^2$) | $R^2$ train. (–) | $R^2$ val. (–) |
|---|---|---|---|---|---|
| 1 | 5 | 28.03 | 27.63 | 0.9870 | 0.9882 |
| 2 | 10 | 27.56 | 27.37 | 0.9874 | 0.9884 |
| 3 | **15** | 27.35 | **27.36** | 0.9876 | **0.9884** |
| 4 | 20 | **27.21** | 27.36 | **0.9877** | 0.9884 |

**Table 6**
Model's results for training and validation steps with detail series $d(1)$.

| Configuration | Neurons | RMSE train. (W/m$^2$) | RMSE val. (W/m$^2$) | $R^2$ train. (–) | $R^2$ val. (–) |
|---|---|---|---|---|---|
| 1 | **5** | 29.33 | **28.50** | 0.0198 | **0.0051** |
| 2 | 10 | **29.33** | 28.53 | **0.0204** | 0.0032 |
| 3 | 15 | 29.37 | 28.56 | 0.0176 | 0.0015 |
| 4 | 20 | 29.37 | 28.62 | 0.0172 | 0.0014 |

**Table 7**
Model's results for training and validation steps with detail series $d(2)$.

| Configuration | Neurons | RMSE train. (W/m$^2$) | RMSE val. (W/m$^2$) | $R^2$ train. (–) | $R^2$ val. (–) |
|---|---|---|---|---|---|
| 1 | 5 | 23.89 | 22.43 | 0.4911 | 0.4785 |
| 2 | **10** | 23.69 | **22.43** | 0.4993 | **0.4786** |
| 3 | 15 | **23.56** | 22.48 | **0.5048** | 0.4767 |
| 4 | 20 | 23.59 | 22.59 | 0.5038 | 0.4713 |

**Table 8**
Model's results for training and validation steps with detail series $d(3)$.

| Configuration | Neurons | RMSE train. (W/m$^2$) | RMSE val. (W/m$^2$) | $R^2$ train. (–) | $R^2$ val. (–) |
|---|---|---|---|---|---|
| 1 | 5 | 19.73 | 19.99 | 0.7520 | 0.7474 |
| 2 | **10** | 19.56 | **19.95** | 0.7563 | **0.7486** |
| 3 | 15 | 19.45 | 19.99 | 0.7588 | 0.7475 |
| 4 | 20 | **19.40** | 20.02 | **0.7602** | 0.7467 |

RMSE and maximizes the $R^2$ structures in the validation step will be chosen.

Finally, after the combination of the results provided by the optimized structures for each approximation and detail series, the accuracy of the proposed forecaster was analysed. Concerning RMSE evolution, proposed model improves it from 59.47 W/m$^2$ to 36.93 W/m$^2$ and from 57.25 W/m$^2$ to 35.77 W/m$^2$ in training and validation steps, respectively. In terms of RMSE percentage evolution, the accuracy increases 37.90% and 37.52% in training and validation steps respectively. Concerning $R^2$ metric the evolution was from 0.9446 to 0.9786 and 0.9518 to 0.9812 in learning and validation databases, respectively. Fig. 5 shows the evolution of solar irradiation's actual and forecasted values for June 16, 2017 for proposed forecaster with Daubechies wavelet transform. While the RMSE calculated for this sample day was 32.80 W/m$^2$; which means an accuracy improvement of 8.64% compared against the persistence model, the $R^2$ error metric improves from 0.9903 to 0.9916.

*3.1.2.3. Discussion between Daubechies and Haar wavelet time-frequency forecasters results.* Although it is true that both analysed wavelet time-frequency transformations have increased forecasters' accuracy, there is little difference between them. While Haar transform obtains 35.81 W/m$^2$ in the validation step, Daubechies obtains 35.77 W/m$^2$ for same step. However, if the random example day is examined it can be seen how Haar transformation obtains 31.70 W/m$^2$ and Daubechies transformation obtains 32.80 W/m$^2$. Therefore, in order to ensure that proper transformation is chosen, ten random days under different meteorological situations were examined. Table 9 summarizes the results of these tests.

After examining the results presented in Table 9, it has been concluded that there is little difference between both wavelet time-frequency transformations. In addition, it cannot be concluded which of the wavelet transforms produces better predictions under each of the examined meteorological situations. Under any meteorological situation, half of the examined random sample days get better prediction with one wavelet transformation and the other half of the examined random days with the other wavelet transformation. Finally, Daubechies transformation was chosen for final forecaster's development as it performs slightly better than Haar transformation. Daubechies RMSE for the validation database was 35.77 W/m$^2$, whereas Haar RMSE for same database was 35.81 W/m$^2$. Concerning to the computational cost, the averaged computation time for each prediction was 0.83 ms, so taking into account that predictios were done for 10 min ahead, the computation time can be consider quick enough.

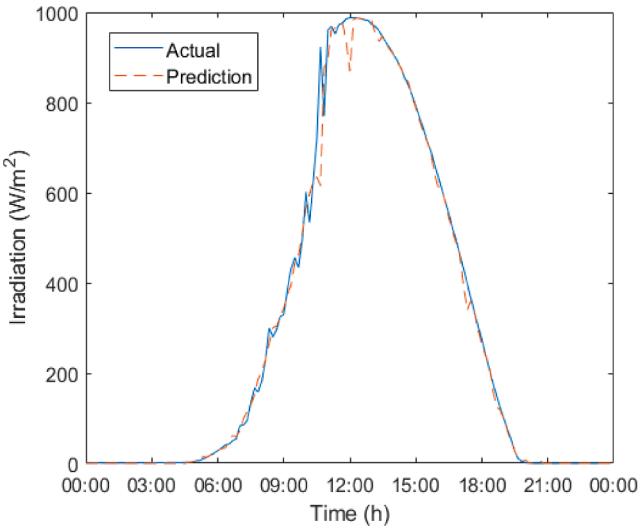


**Fig. 5.** Actual and forecasted values for June 16, 2017.

**Table 9**
RMSE calculated for different situations by each proposed model.

| | | Haar Transformation | Daubechies Transformation |
|---|---|---|---|
| **Type of Day** | **Date** | **RMSE (W/m$^2$)** | **RMSE (W/m$^2$)** |
| Sunny | 05/01/2017 | **7.49** | 8.19 |
| | 08/01/2017 | **8.66** | 8.72 |
| | 10/03/2017 | **6.41** | 6.79 |
| | 12/04/2017 | **9.96** | 10.04 |
| | 17/06/2017 | 7.18 | **7.12** |
| | 21/08/2017 | 7.18 | **5.43** |
| | 11/10/2017 | 4.46 | **3.86** |
| | 26/10/2017 | 4.97 | **4.06** |
| | 20/11/2017 | 8.50 | **8.38** |
| | 22/11/2017 | 5.69 | **5.05** |
| Partially cloudy | 04/01/2017 | **10.11** | 10.38 |
| | 09/02/2017 | **24.50** | 24.78 |
| | 22/02/2017 | **16.33** | 16.91 |
| | 09/03/2017 | **14.47** | 14.89 |
| | 03/04/2017 | 20.68 | **20.65** |
| | 25/05/2017 | 20.06 | **19.72** |
| | 19/06/2017 | 14.68 | **14.00** |
| | 22/08/2017 | 21.24 | **20.57** |
| | 15/10/2017 | **18.86** | 19.08 |
| | 06/12/2017 | **10.55** | 11.08 |
| Cloudy | 20/02/2017 | **24.21** | 24.85 |
| | 23/03/2017 | 51.70 | **51.17** |
| | 27/03/2017 | **56.51** | 57.69 |
| | 06/04/2017 | 57.72 | **56.35** |
| | 14/05/2017 | 63.28 | **62.80** |
| | 21/05/2017 | **58.31** | 60.05 |
| | 02/06/2017 | 68.48 | **66.83** |
| | 18/08/2017 | **42.65** | 44.62 |
| | 02/09/2017 | 52.94 | **49.19** |
| | 02/11/2017 | **28.93** | 29.09 |

Figs. 6, 7 and 8 present how proposed forecaster's solar irradiation predictions follow actual values under the different meteorological situation presented in Table 9.

For being able to contrast the accuracy of predictions done by the developed forecaster against literature's results, MAE error metric was also computed. While Table 10 contains the averaged ($\mu$), deviation ($\sigma$), maximum (*Max.*) and minimum (*Min.*) values of the error metrics computed for the random days presented in Table 9 through Daubechies wavelet transform, Fig. 9 contains a 3D pie chart diagram to show the error percentage distribution of all 2017 days. Fig. 9 shows that for

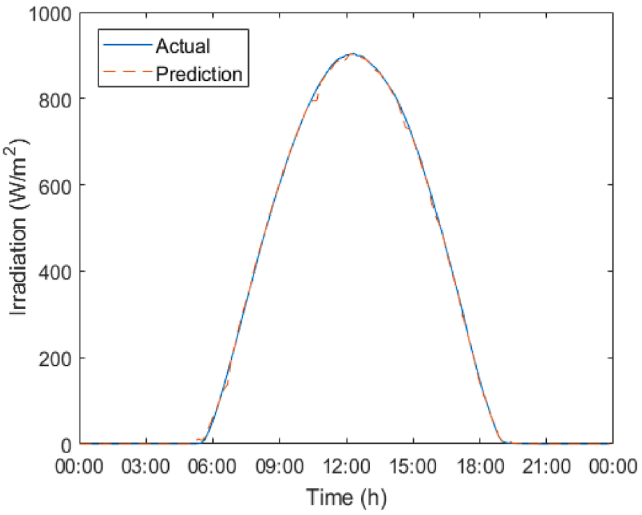


**Fig. 6.** Actual vs. forecasted values for a sunny day, August 21, 2017.

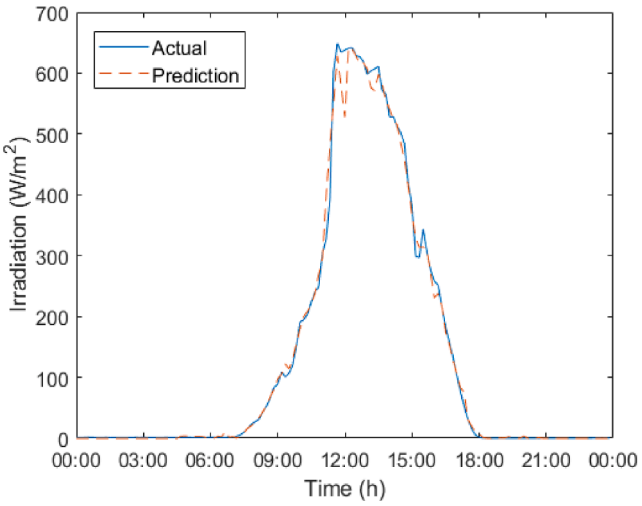


**Fig. 7.** Actual vs. forecasted values for a partially cloudy day, February 22, 2017.

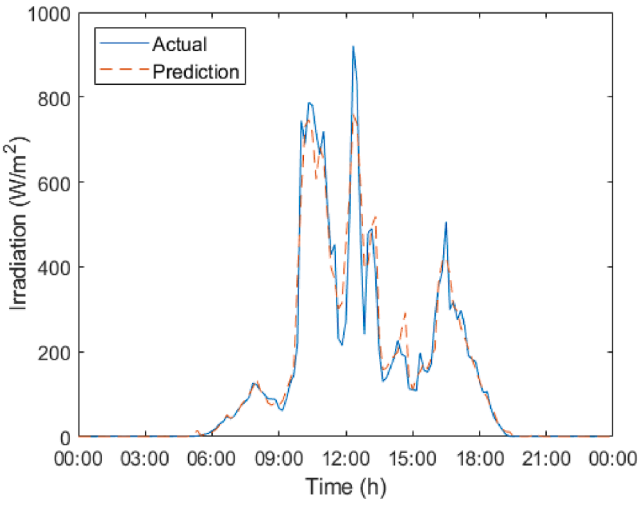


**Fig. 8.** Actual vs. forecasted values for a cloudy day, August 18, 2017.

**Table 10**
Daubechies wavelet time-frequency forecaster's error metrics.

| Type of Day | Parameter | RMSE (W/m$^2$) | $R^2$ (–) | MAE (W/m$^2$) |
|---|---|---|---|---|
| Sunny | Average | 6.76 | 0.9993 | 3.25 |
| | Deviation | 1.99 | 0.0005 | 0.86 |
| | Max | 10.04 | 0.9998 | 4.66 |
| | Min | 3.86 | 0.9984 | 1.93 |
| Partially Cloudy | Average | 17.21 | 0.9950 | 7.30 |
| | Deviation | 4.36 | 0.0020 | 1.80 |
| | Max | 24.78 | 0.9976 | 10.76 |
| | Min | 10.38 | 0.9915 | 4.93 |
| Cloudy | Average | 50.26 | 0.9630 | 22.63 |
| | Deviation | 13.22 | 0.0099 | 5.84 |
| | Max | 66.83 | 0.9832 | 29.67 |
| | Min | 24.85 | 0.9502 | 11.04 |

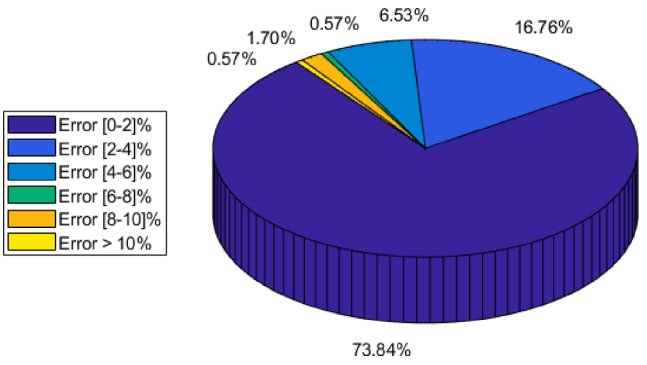


**Fig. 9.** Cumulative error pie chart distribution of the examined days on 2017.

90.60% of 2017′s days, the cumulative error between actual and forecasted solar irradiation values is lower than 4%. In addition, only for the 0.57% of 2017′s days, the deviation is greater than the 10%.

Once Daubechies transformation has been chosen for the development of the final forecaster and some random sample days were computed under different meteorological situations, next step consists of contrasting obtained accuracy metric results against literature results [35,57,58]. Although [35] is a previous study where same database was used, studies [57,58] were computed with different databases. Therefore, the comparison between developed forecaster and literature forecasters will be done analyzing computed error metrics in terms of whole year or by meteorological situations, i.e. sunny, partially cloudy or cloudy.

In previous study [35] a spatio-temporal FFNN forecaster was developed. Spatio-temporal technique consists in taking into account not only the relevant information of target location but also surrounding stations information to develop the final forecaster. If the results of both forecasters are compared, it can be seen how the forecaster based on Daubechies transformation reduces spatio-temporal FFNN forecaster's RMSE value from 50.80 W/m$^2$ to 35.77 W/m$^2$, which means an accuracy improvement of 25.59%. Moreover, if forecasters' performances under different meteorological conditions are compared, it is demonstrated that Daubechies forecasters produces better predictions. For same examined sunny days spatio-temporal forecaster gets a RMSE range from 5.11 to 16.93 W/m$^2$ with an averaged and standard deviation RMSE values of 9.34 W/m$^2$ and 3.83 W/m$^2$, respectively; Daubechies forecaster gets a range from 3.86 to 10.04 W/m$^2$ with an averaged and standard deviation RMSE values of 6.76 W/m$^2$ and 2.10 W/m$^2$, respectively. For same examined partially cloudy days spatio-temporal forecaster gets a RMSE range from 19.50 to 39.92 W/m$^2$ with an averaged and standard deviation RMSE values of 28.13 W/m$^2$ and 5.87 W/m$^2$, respectively; Daubechies forecaster gets a range from 10.38 to 24.78 W/m$^2$ with an averaged and standard deviation RMSE values of 17.89 W/m$^2$ and 4.31 W/m$^2$, respectively. Finally, for same examined cloudy days, spatio-temporal forecaster gets a RMSE range from 32.47 to 83.89 W/m$^2$ with an averaged and standard deviation RMSE values of 67.40 W/m$^2$ and 16.32 W/m$^2$, respectively; Daubechies forecaster gets a range from 24.85 to 66.83 W/m$^2$ with an averaged and standard deviation RMSE values of 50.26 W/m$^2$ and 13.93 W/m$^2$, respectively. Therefore, based on obtained results it can be concluded that the introduction of Daubechies wavelet time-frequency transformation increases forecaster's accuracy. Developed Daubechies forecaster in this study only takes into account target location's data, following studies will examine whether combining Daubechies and spatio-temporal forecasters final accuracy is increased.

In other research, Caldas et al. [57] proposed a solar irradiance hybrid forecaster which is based on the combination of sky imagery with real-time values with a prediction horizon range that covers from one to ten minutes. This forecaster uses sky images to detect and compute clouds movement, and combines this information with real-time solar irradiation measurements obtained through a meteorological station to predict clouds impact on solar irradiation in a certain location. Caldas et al. provide error metrics information under same meteorological situations studied in this paper. Hence, focusing on 10 min ahead prediction horizon error metrics, for sunny days Caldas et al.'s forecaster gets an averaged RMSE of 4.4 W/m$^2$ and proposed Daubechies forecaster gets a range from 3.86 to 10.04 W/m$^2$. For cloudy days Caldas et al.'s forecaster gets an averaged RMSE of 110 W/m$^2$ and proposed Daubechies forecaster gets a range from 24.85 to 66.83 W/m$^2$. Finally, for partially cloudy days, Caldas et al.'s forecaster gets an averaged RMSE and MAE of 251 W/m$^2$ and 168 W/m$^2$, respectively and proposed Daubechies forecaster gets a range from 10.38 to 24.78 W/m$^2$ for RMSE and from 4.78 to 11.76 W/m$^2$ for MAE. Obtained results demonstrate that proposed Daubechies forecaster improve Caldas et al.'s forecaster for partially cloudy and cloudy days, whereas similar error metrics are obtained for sunny days.

Wen et al. [58] proposed a multistep forecaster based on assembling several CNNs to predict solar irradiation values from 5 to 10 min ahead with a minute resolution. Although CNN are able to make predictions through the use of historical databases, Wen et al. have proposed to make predictions through the combination of stacked consecutive images. The stacked consecutive images consist of extracting from three consecutive images same colour channel and stacking them maintaining the original order to create a new image that will be used in the forecaster. In this study Wen et al. have demonstrated that this novel concept of stacking consecutive images increases the accuracy of the forecasters in comparison with those forecasters that did not used the stacking consecutive images methodology. Nevertheless, Wen et al. did not provide separate error metrics under different meteorological situations; they only provided the global RMSE of 104 W/m$^2$ for 30 consecutive days including different meteorological conditions and cloud patters. Therefore, if global RMSEs of both forecasters are compared assuming that both metrics have been obtained through the inclusion of different meteorological conditions and cloud patters, it seems that Daubechies forecaster, with 35.77 W/m$^2$ for whole validation 2017 year, makes slightly better predictions.

After contrasting that proposed forecaster based on Daubechies transformation slightly increases literatures' results, PV output power was calculated. To make this calculation, same equation proposed in previous study [35] has been applied,

$$P_{PV}(t) = \eta * S * W(t) * (1 - 0.005 * (T(t) - 25)) \quad (18)$$

Where, $t$ represent time (s), $P_{PV}(t)$ refers to the power generated by PVs ($W$) at each $t$ time, $\eta$ is the efficiency of the PV panels, $S$ is the surface of the PV generator ($m^2$), $W(t)$ is the solar irradiation value ($W/m^2$) at each $t$ time and T(t) is the outdoor ambient temperature ($^{\circ}C$) at each $t$ time. Although it is true that both temperature and solar irradiation vary, Eq. (18) shows that for generated output power parameter temperature effect is lower than solar irradiation's along the day so, it is assumed that

the temperature in this case can be forecasted by persistence model where $T(t) = T(t+10\ \text{min})$. For being able to calculate the output power through Eq. (18), a commercial panel ($\eta = 17.59\%$ and $S = 1.6767\ m^2$) was chosen. Fig. 10a and 10b show the accumulated actual and forecasted power values for sunny and cloudy days.

Fig. 10a shows the evolution of accumulated actual and forecasted energy for a sunny day August 21, 2017, being the deviation at the end of the day 6.3 Wh which means a relative error of 0.33%. Fig. 10b shows the evolution of accumulated actual and forecasted energy for a cloudy day August 18, 2017, being the deviation at the end of the day 19.1 Wh which means a relative error of 1.90%. Moreover, Fig. 10a and 10b demonstrate the difference between sunny and cloud days, while trend in Fig. 10a is smoother due to absence of clouds during all day, Fig. 10b has some bumps due to the presence of clouds that produce sudden changes in PV generation. Finally, the same computation done for days shown in Fig. 10a and 10b has been done with the data from January to August 2017. The result of this analysis is shown in Fig. 11. This period from January to August 2017 has been chosen for being able to compare the results of Daubechies forecaster with the results of previous spatio-temporal forecaster [35].

While Daubechies forecaster presented in this paper gets an accumulated error rate lower than 2% for the 77.35% of analysed days for period January to August 2017, the spatio-temporal forecaster developed in [35] gets to 65.81%. Moreover, the mean error percentage obtained in this study is 1.46%, whereas the error percentage obtained in [35] was 2.40%. Thus, it can be concluded that Daubechies forecaster produces better solar irradiation predictions than the spatio-temporal forecaster developed in [35].

## 4. Conclusions

The aim of this study was to present the developed solar irradiation forecaster which provides predictions 10 min ahead in order to compute solar PV generators production. Based on obtained error metrics results and after contrasting them against literature results, this forecaster can be used to reduce PV generators' uncertainty level to make them more reliable. Main contributions of this research are:

- Two different wavelet time-frequency transformations, Haar and Daubechies, have been examined in order to predict solar irradiation parameter 10 min ahead. Both wavelet transformations produce similar error metrics. Finally, based on the global RMSE in the validation step, 35.77 W/m$^2$, Daubechies wavelet transform has been chosen for the final forecaster development.
- Proposed forecaster consists of making a Daubechies wavelet time-frequency transformation in order to transform original solar irradiation data series into a combination of four series, an approximation series and three detailed series. Each of these series has been used to develop a FFNN model whose predictions are combined to produce final global prediction. This model gets RMSEs of 36.93 W/m$^2$ and 35.77 W/m$^2$ in training and validation steps, which means an accuracy improvement 37.90% and 37.52% when they are contrasted with persistence benchmark forecaster.
- Daubechies forecaster developed in this study has also been compared against a previously developed spatio-temporal FFNN forecaster [35]. It has been demonstrated that Daubechies wavelet transforms increases forecaster accuracy from 50.80 W/m$^2$ to 35.77 W/m$^2$ in terms of RMSE in the validation step for whole 2017, which means an accuracy improvement of 25.59%. In addition, the mean error cumulative percentage obtained in this study is 1.46%, whereas the error percentage obtained in spatio-temporal FFNN forecaster was 2.40% for period January to August 2017. Developed forecaster has also been compared against some literature forecasters such as Wen et al. [58]. While the RMSE of Wen et al. forecaster was 104 W/m$^2$ for examined period of time under different weather conditions, developed forecaster's RMSE was 35.77 W/m$^2$ under different weather conditions. Therefore, it can be concluded that developed forecaster makes more accurate predictions.
- All the calculations done and the results presented in this study are based on real data from a meteorological station located in Vitoria-Gasteiz, Spain. While data from 2015 to 2016 has been applied for training step, data from 2017 has been used for validation step in order to ensure that forecasters do not previously seen this data in training step. Although it has been demonstrated that Daubechies transformation increases forecasters' accuracy, it will be necessary to fix the number of neurons of FFNNs if data of other locations is used. This step is relevant in order to ensure the maximum accuracy.

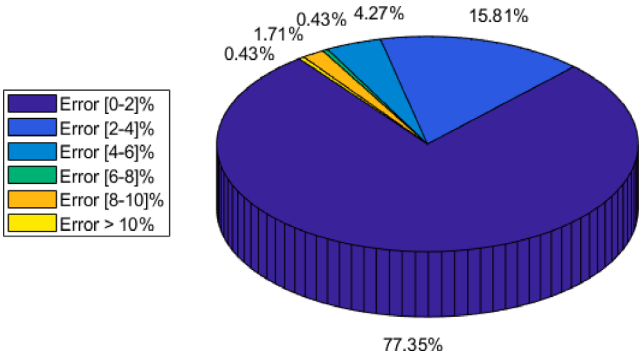


**Fig. 11.** Cumulative error distribution for period January to August 2017

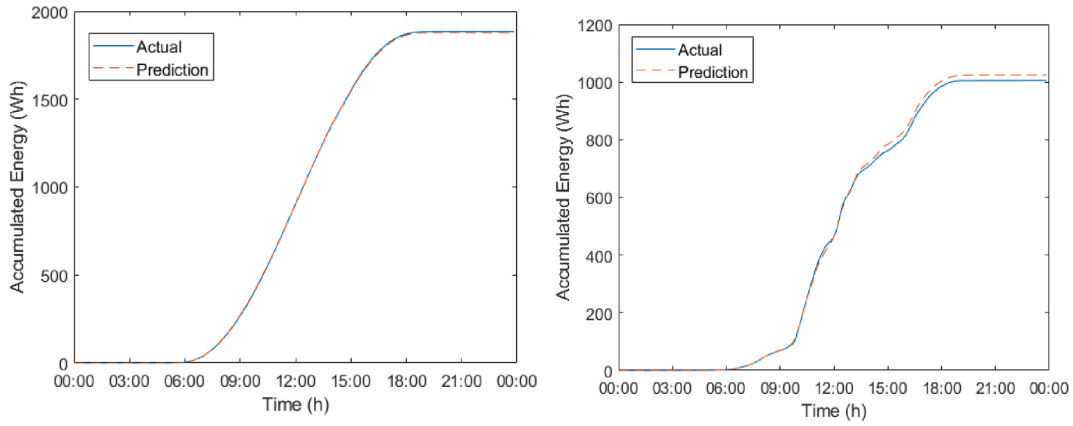


**Fig. 10.** Actual vs. forecasted accumulated energy for a) sunny day, August 22, 2017 (left) and b) cloudy day, August 18, 2017 (right).

*CRediT authorship contribution statement*

**Fermín Rodríguez:** Conceptualization, Methodology, Validation, Resources, Investigation, Writing – original draft. **Iñigo Azkarate:** Methodology, Software, Resources, Investigation, Writing – review & editing. **Javier Vadillo:** Formal analysis, Supervision, Writing – review & editing. **Ainhoa Galarza:** Conceptualization, Visualization, Writing – review & editing.

## Declaration of Competing Interest

The authors declare that they have no known competing financial interests or personal relationships that could have appeared to influence the work reported in this paper.

## Acknowledgements

The authors would like to thank the Basque Government's Department of Education for financial support through the Researcher Formation Programme; grant number PRE_2020_2_0038.

## References

[1] Alarenan S, Gasim AA, Hunt LC. Modelling industrial energy demand in Saudi Arabia. Energy Econo 2020;85:104554. https://doi.org/10.1016/j.eneco.2019.104554.
[2] Liu J, Niu D, Song X. The energy supply and demand pattern of China: A review of evolution and sustainable development. Renew Sustain Energy Rev 2013;25:220–8. https://doi.org/10.1016/j.rser.2013.01.061.
[3] Goldemberg J. The evolution of the energy and carbon intensities of developing countries. Energy Pol 2020;137:1060. https://doi.org/10.1016/j.enpol.2019.111060.
[4] Afroz Z, Urmee T, Shafiullah GM, Higgins G. Real-time prediction model for indoor temperature in a commercial building. Appl Energy 2018;231:29–53. https://doi.org/10.1016/j.apenergy.2018.09.052.
[5] Ayvazoğluyüksel Ö, Filik ÜB. Estimation methods of global solar irradiation, cell temperature and solar power forecasting: A review and a case study in Eskişehir. Renew Sustain Energy Rev 2018;91:639–53. https://doi.org/10.1016/j.rser.2018.03.084.
[6] Lotta MC, Pye S, Dodds PE. Quantifying the co-impacts of energy sector decarbonisation on outdoor air pollution in the United Kingdom. Energy Policy 2017;101:42–51. https://doi.org/10.1016/j.enpol.2016.11.028.
[7] IEA, Trends 2018 in Photovoltaic Applications - IEA-PVPS. http://www.iea-pvps.org/fileadmin/dam/intranet/task1/IEA_PVPS_Trends_2018_in_Photovoltaic_Applications.pdf [accessed 19 November 2019].
[8] REN21, advancing the global renewable energy transition. https://www.ren21.net/wp-content/uploads/2019/08/Highlights-2018.pdf [accessed 25 November 2019].
[9] Marchesoni-Acland F, Alonso-Suárez R. Intra-day solar irradiation forecast using RLS filters and satellite images. Renew Energy 2020;161:1140–54. https://doi.org/10.1016/j.renene.2020.07.101.
[10] Notton G, Nivet M-L, Voyant C, Paoli C, Darras C, Motte F, et al. Intermittent and stochastic character of renewable energy sources: consequences, cost of intermittence and benefit of forecasting. Renew Sustain Energy Rev 2018;87:96–105. https://doi.org/10.1016/j.rser.2018.02.007.
[11] Rodríguez F, Genn M, Fontán L, Galarza A. Very short-term temperature forecaster using MLP and N-nearest stations for calculating key control parameters in solar photovoltaic generation. Sustainable Energy Technol Assess 2021;45:101085. https://doi.org/10.1016/j.seta.2021.101085.
[12] Alahyari A, Ehsan M, Mousavizadeh M. A hybrid storage-wind virtual power plant (VPP) participation in the electricity markets: A self-scheduling optimization considering price, renewable generation, and electric vehicles uncertainties. J Energy Storage 2019;25:100812. https://doi.org/10.1016/j.est.2019.100812.
[13] Adu-Kankamab KO, Camarinha-Matosa C. Towards collaborative virtual power plants: trends and convergence. Sustain Energy Grids Netw 2018;16:217–30. https://doi.org/10.1016/j.segan.2018.08.003.
[14] Wen L, Zhou K, Yang S, Lu X. Optimal load dispatch of community microgrid with deep learning based solar power and load forecasting. Energy 2019;171:1053–65. https://doi.org/10.1016/j.energy.2019.01.075.
[15] https://www.eleconomista.es/empresas-finanzas/noticias/10946004/12/20/Naturgy-instala-un-sistema-pionero-en-Espana-de-baterias-en-parques-eolicos.html [accessed 01/02/2021].
[16] https://www.sciencemag.org/news/2019/07/giant-batteries-and-cheap-solar-power-are-shoving-fossil-fuels-grid [accessed 08/02/2021].
[17] Sobri S, Koohi-Kamali S, Rahim NA. Solar photovoltaic generation forecasting methods: a review. Energy Conv Manag 2018;156:459–97. https://doi.org/10.1016/j.enconman.2017.11.019.
[18] Agüera-Pérez A, Palomares-Salas JC, Rosa JJG, Florencias-Oliveros O. Weather forecasts for microgrid energy management: Review, discussion and recommendations. Appl Energy 2018;2018(228):265–78. https://doi.org/10.1016/j.apenergy.2018.06.087.
[19] Antonopoulos I, Robu V, Couraud B, Kirli D, Norbu S, Kiprakis A, et al. Artificial intelligence and machine learning approaches to energy demand-side response: A systematic review. Renew Sust Energy Rev 2020;130:109899. https://doi.org/10.1016/j.rser.2020.109899.
[20] Li Z, Rahman SMM, Vega R, Dong B. A Hierarchical Approach Using Machine Learning Methods in Solar Photovoltaic Energy Production Forecasting. Energies 2016;9(1):55. https://doi.org/10.3390/en9010055.
[21] Antonanzas J, Osorio N, Escobar R, Urraca R, Martinez-de-Pison FJ, Antonanzas-Torres F. Review of photovoltaic power forecasting. Sol Energy 2016;136:78–111. https://doi.org/10.1016/j.solener.2016.06.069.
[22] Zhang J, Verschae R, Nobuhara S, Lalonde JF. Deep photovoltaic nowcasting. Sol Energy 2018;176:267–76. https://doi.org/10.1016/j.solener.2018.10.024.
[23] Chen X, Du Y, Lim E, Wen H, Jiang L. Sensor network based PV power nowcasting with spatio-temporal preselection for grid-friendly control. Appl Energy 2019;255:113760. https://doi.org/10.1016/j.apenergy.2019.113760.
[24] Chu Y, Li M, Coimbra CFM. Sun-tracking imaging system for intra-hour DNI forecasts. Renew Energy 2016;96:792–9. https://doi.org/10.1016/j.renene.2016.05.041.
[25] Jamal T, Carter C, Schmidt T, Shafiullah GM, Calais M, Urmee T. An energy flow simulation tool for incorporating short-term PV forecasting in a diesel-PV-battery off-grid power supply system. Appl Energy 2019;254:113718. https://doi.org/10.1016/j.apenergy.2019.113718.
[26] Amanpreet K, Nonnenmacher L, Pedro HTC, Coimbra CFM. Benefits of solar forecasting for energy imbalance markets. Renew Energy 2016;86:819–30. https://doi.org/10.1016/j.renene.2015.09.011.
[27] David M, Luis MA, Lauret P. Comparison of intraday probabilistic forecasting of solar irradiance using only endogenous data. Int J Forecast 2018;34(3):529–47. https://doi.org/10.1016/j.ijforecast.2018.02.003.
[28] Aguiar LM, Pereira B, Lauret P, Díaz F, David M. Combining solar irradiance measurements, satellite-derived data and a numerical weather prediction model to improve intra-day solar forecasting. Renew Energy 2016;97:599–610. https://doi.org/10.1016/j.renene.2016.06.018.
[29] Sperati S, Alessandrini S, Delle Monache L. An application of the ECMWF Ensemble Prediction System for short-term solar power forecasting. Sol Energy 2016;133:437–50. https://doi.org/10.1016/j.solener.2016.04.016.
[30] Araya IA, Valle C, Allende H. A Multi-Scale Model based on the Long Short-Term Memory for day ahead hourly wind speed forecasting [in press] Pattern Recognit Lett 2019. https://doi.org/10.1016/j.patrec.2019.10.011.
[31] Gürter M, Paulsen T. The effect of wind and solar power forecasts on day-ahead and intraday electricity prices in Germany. Energy Econ 2018;75:150–62. https://doi.org/10.1016/j.eneco.2018.07.006.
[32] Chazarra M, Pérez-Díaz JI, García-González J, Helseth A. Economic effects of forecasting inaccuracies in the automatic frequency restoration service for the day-ahead energy and reserve scheduling of pumped storage plants. Electr Power Syst Res 2019;174:105850. https://doi.org/10.1016/j.epsr.2019.04.028.
[33] Aguiar LM, Polo J, Vindel JM, Oliver A. Analysis of satellite derived solar irradiance in islands with site adaptation techniques for improving the uncertainty. Renew Energy 2019;135:98–107. https://doi.org/10.1016/j.renene.2018.11.099.
[34] Dupré A, Dobrinski P, Alnzo B, Bados J, Briad C, Plougoven R. Sub-hourly forecasting of wind speed and wind energy. Renew Energy 2020;145:2373–9. https://doi.org/10.1016/j.renene.2019.07.161.
[35] Rodríguez F, Martín F, Fontán L, Galarza A. Ensemble of machine learning and spatiotemporal parameters to forecast very short-term solar irradiation to compute photovoltaic generators' output power. Energy 2021;229:120647. https://doi.org/10.1016/j.energy.2021.120647.
[36] Aasim, Singh SN, Mohapatra A. Repeated wavelet transform based ARIMA model for very short-term wind speed forecasting. Renew Energy 2019;136:758–68. https://doi.org/10.1016/j.renene.2019.01.031.
[37] David M, Ramahatana F, Trombe PJ, Lauret P. Probabilistic forecasting of the solar irradiance with recursive ARMA and GARCH models. Sol Energy 2016;133:55–72. https://doi.org/10.1016/j.solener.2016.03.064.
[38] Liu M, Cao Z, Zhang J, Wang L, Huang C, Luo X. Short-term wind speed forecasting based on the Jaya-SVM model. Int J Electr Power Energy Syst 2020;121:106056. https://doi.org/10.1016/j.ijepes.2020.106056.
[39] Rodríguez F, Martín F, Fontán L, Galarza A. Very Short-Term Load Forecaster Based on a Neural Network Technique for Smart Grid Control. Energies 2020;13(19):5210. https://doi.org/10.3390/en13195210.
[40] Liu Y, Qin H, Zhang Z, Pei S, Wang C, Yu X, et al. Ensemble spatiotemporal forecasting of solar irradiation using variational Bayesian convolutional gate recurrent unit network. Appl Energy 2019;253:113596. https://doi.org/10.1016/j.apenergy.2019.113596.
[41] Shireen T, Shao C, Wang H, Li J, Zhang X, Li M. Iterative multi-task learning for time-series modeling of solar panel PV outputs. Appl Energy 2018;212:654–62. https://doi.org/10.1016/j.apenergy.2017.12.058.
[42] Lan H, Zhang C, Hong YY, He Y, Wen S. Day-ahead spatiotemporal solar irradiation forecasting using frequency-based hybrid principal component analysis and neural network. Appl Energy 2019;247:389–402. https://doi.org/10.1016/j.apenergy.2019.04.056.
[43] Wang K, Qi X, Liu H. A comparison of day-ahead photovoltaic power forecasting models based on deep learning neural network. Appl Energy 2019;251:113315. https://doi.org/10.1016/j.apenergy.2019.113315.
[44] Zhao X, Jiang N, Liu J, Daren Y, Chang J. Short-term average wind speed and turbulent standard deviation forecasts based on one-dimensional convolutional

neural network and the integrate method for probabilistic framework. Energy Conv Manage 2020;203:112239. https://doi.org/10.1016/j.enconman.2019.112239.
[45] Chen Y, Zhang S, Zhang W, Peng J, Cai Y. Multifactor spatio-temporal correlation model based on a combination of convolutional neural network and long short-term memory neural network for wind speed forecasting. Energy Conv Manage 2019;185:783–99. https://doi.org/10.1016/j.enconman.2019.02.018.
[46] Germoui M, Melgani F, Gairaa K, Lamine-Mekhalfi M. A comprehensive review of hybrid models for solar radiation forecasting. J Clean Prod 2020;258:120357. https://doi.org/10.1016/j.jclepro.2020.120357.
[47] Ghimire S, Deo RC, Raj N, Mi J. Deep solar radiation forecasting with convolutional neural network and long short-term memory network algorithms. Appl Energy 2019;235:113541. https://doi.org/10.1016/j.apenergy.2019.113541.
[48] Feng C, Zhang J. Hourly-Similarity Based Solar Forecasting Using Multi-Model Machine Learning Blending; 2018. https://ieeexplore.ieee.org/xpl/conhome/8540807/proceeding.
[49] Li S, Ma H, Li W. Typical solar radiation year construction using k-means clustering and discrete-time Markov chain. Appl Energy 2017;205:720–31. https://doi.org/10.1016/j.apenergy.2017.08.067.
[50] Baser F, Demirhan H. A fuzzy regression with support vector machine approach to the estimation of horizontal global solar radiation. Energy 2017;123(229-240). https://doi.org/10.1016/j.energy.2017.02.008.
[51] Li K, Wang R, Lei H, Zhang T, Liu Y, Zheng X. Interval prediction of solar power using an improved bootstrap method. Sol Energy 2018;159:97–112. https://doi.org/10.1016/j.solener.2017.10.051.
[52] Liu L, Zhao Y, Chang D, Xie J, Ma Z, Sun Q, et al. Prediction of short-term PV power output and uncertainty analysis. Appl Energy 2018;228:700–11. https://doi.org/10.1016/j.apenergy.2018.06.112.
[53] Rodríguez F, Bazmohammadi N, Guerrero JM, Galarza A. A Very Short-Term Probabilistic Prediction Interval Forecaster for Reducing Load Uncertainty Level in Smart Grids. Appl Sci 2021;11(6):2538. https://doi.org/10.3390/app11062538.
[54] Zhu Y, Zhang C, Zhou D, Wang Y, Bai X, Liu W. Traffic sign detection and recognition using fully convolutional network guided proposals. Neurocomp 2016;214:758–66. https://doi.org/10.1016/j.neucom.2016.07.009.
[55] Haykin S. Neural Networks and Learning Machines, 3rd edition. Pearson Education, Inc, Upper Saddle River. McMaster University, Ontario Canada; 2009.
[56] Kalogirou SA. Artificial neural networks in renewable energy systems applications: a review. Renew Sustain Energy Rev 2001;5:373–401. https://doi.org/10.1016/S1364-0321(01)00006-5.
[57] Caldas M, Alonso-Suárez R. Very short-term solar irradiance forecast using all-sky imaging and real time measurements. Renew Energy 2019;143:1643–58. https://doi.org/10.1016/j.renene.2019.05.069.
[58] Wen H, Du Y, Chen X, Lim E, Wen H, Jiang L, et al. Deep Learning Based Multistep Solar Forecasting for PV Ramp-Rate Control Using Sky Images. IEEE Transac Indus Infor 2021;17(2):1397–406. https://doi.org/10.1109/TII.2020.2987916.